

## Evolution of Hydrogen Platelets in Silicon Determined by Polarized Raman Spectroscopy

E. V. Lavrov\* and J. Weber

University of Technology, 01062 Dresden, Germany  
(Received 14 July 2001; published 15 October 2001)

Crystalline silicon treated in a remote hydrogen plasma exhibits  $\{111\}$  platelike defects. From polarized Raman spectroscopy, we identify two different hydrogen-related extended  $\{111\}$  defects, which exist simultaneously in the samples: an optically dense structure with  $\epsilon \cong 14$  and a structure with  $\epsilon \cong 1$  which contains the  $H_2$  molecules. The platelet with  $\epsilon \cong 14$  is assigned to agglomerated  $H_2^*$  defects in a (111) plane. At 100 °C, it transforms into the platelet with  $\epsilon \cong 1$ , which is assigned to hydrogenated silicon (111) surfaces.

DOI: 10.1103/PhysRevLett.87.185502

PACS numbers: 61.72.Ji, 61.72.Nn, 78.30.Am

The precipitation of high hydrogen concentrations in crystalline silicon results in ordered planar defects called platelets. The formation process and the structure of these extended defects is at present the subject of intense discussion [1,2]. The dominant platelets created by hydrogen plasma treatment are those lying in  $\{111\}$  planes [3]. Based on electron microscopy studies [4], Raman scattering [5], as well as infrared absorption [5], it has been established that the basic units comprising these platelets are Si—H bonds. A number of different structural models of the platelets have been suggested based on both theoretical and experimental investigations. From high-resolution transmission electron microscopy studies, it has been suggested that the  $\{111\}$  platelet is a H-saturated internal (111) surface structure  $[2Si—H]_n$ , i.e., the configuration in which each Si—Si bond in an (111) plane is replaced by two Si—H bonds [4]. However, theory has shown that this structure is not stable against the formation of hydrogen molecules at tetrahedral interstitial,  $T$ , sites [6,7]. On the other hand, recent experiments on the dependence of the platelet concentration on the position of the Fermi level suggest that  $H_2^*$  aggregates are involved in the formation of the  $\{111\}$  platelets [8]. This model is in agreement with calculations by Zhang and Jackson, who found that the double layer of  $H_2^*$ ,  $[H_2^*]_n^D$ , has the lowest energy of all proposed models for the  $\{111\}$  platelets [9]. Thus, there appears to be two types of platelets.

In this Letter, we present the detailed analysis of polarized Raman scattering spectra measured on the  $\{111\}$  hydrogen platelets in Si hydrogenated by remote plasma exposure. The first Raman scattering study by Heyman *et al.* [5] showed that Raman active modes of the  $\{111\}$  platelets are observed at approximately  $2100\text{ cm}^{-1}$  and transform according to the fully symmetric representation of a trigonal point group. Recent Raman scattering studies of hydrogenated Si by Leitch *et al.* [10] showed that platelets may trap  $H_2$ , with a local vibrational mode at  $4160\text{ cm}^{-1}$ . Our analysis of the  $2100\text{-}$  and  $4160\text{-cm}^{-1}$  bands identifies the two different types of platelets described above, which coexist in concentrations depending on the plasma conditions.

Silicon samples used in this study were  $n$ -type, phosphorus-doped, Cz (100) wafers with resistivity of  $0.75\ \Omega\text{ cm}$ . Hydrogen was introduced into the samples by means of a remote dc plasma system. The sample temperature varied from room temperature to 300 °C and annealing time from 30 min to 6 h. The samples were mounted on a heater stage, which was located downstream from the plasma. The temperature was monitored by a thermocouple mounted next to the sample. No effect of the plasma on the thermocouple temperature was measured. The hydrogen pressure was held constant at 1 mbar.

Raman measurements were performed with the 488 nm line of an Ar-ion laser for excitation. The focused incident laser beam made an angle of  $40^\circ$  with the sample normal. The laser power was  $\sim 300\text{ mW}$  and the spot size on the sample surface was  $50\ \mu\text{m}$ . The backscattered light was dispersed using a 0.3 m single grating spectrometer and detected with a cooled Si CCD detector array, whose sensitivity over the whole spectroscopic region of interest remained constant within 5%. Positions of the lines in the spectra were calibrated by the Raman lines of atmospheric  $N_2$ ,  $O_2$ , and  $H_2O$ . The spectral resolution was  $7\text{ cm}^{-1}$ . An appropriate holographic notch filter was used to reduce the scattered laser light. Polarized Raman spectra were collected in a pseudobackscattering geometry. The polarization geometry is defined with respect to the sample surface (100): The  $x$ ,  $y$ , and  $z$  axes are parallel to [100], [010], and [001], while  $y'$  and  $z'$  axes are parallel to [011] and  $[0\bar{1}1]$ . In the notation  $\{a[b, c]d\}$ ,  $a(d)$  refers to the propagation vector of the incident (scattered) light, while  $b(c)$  refers to the polarization vector of the incident (scattered) light. The depolarization ratio,  $\Delta$ , is defined as the ratio of the scattered light intensity polarized perpendicular to the excitation light,  $E^{\text{in}}$ , to the intensity parallel to  $E^{\text{in}}$ . In the notation  $\Delta_{[xyz]}$ , the subscript implies that the excitation light is polarized along the  $[xyz]$  axis. Polarized spectra were corrected for differences in grating efficiency by calibration with a blackbody source.

Figure 1 shows room-temperature, polarization-sensitive spectra of a Si sample after exposure to hydrogen plasma at 150 °C for 6 h. The broadband at  $2100\text{ cm}^{-1}$  was

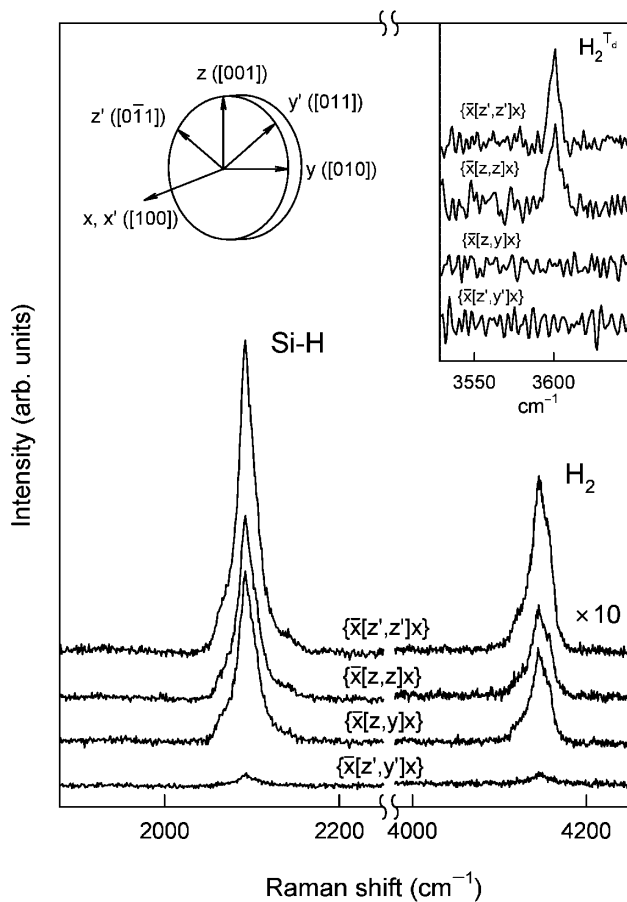


FIG. 1. Room temperature polarized Raman spectra after exposure to a hydrogen plasma at 150°C for 6 h. Polarization geometry is defined with respect to the sample normal [100]. Spectra are offset vertically for clarity. The intensity in the spectral range 1900–4300  $\text{cm}^{-1}$  was scaled up by a factor of 10. The inset shows room temperature polarized Raman spectra of the  $\text{H}_2$  molecule at the  $T$  site.

previously assigned to the  $\{111\}$  platelets [5], whereas the band lying at 4160  $\text{cm}^{-1}$  was associated with  $\text{H}_2$  trapped within platelets [10]. The polarized spectra of the 2100- $\text{cm}^{-1}$  band shown in the figure are in qualitative agreement with previous data reported by Heyman *et al.* [5], i.e.,  $\Delta_{[110]}$  is close to zero, which suggests the fully symmetric mode of a trigonal defect [11]. Note that nonzero intensity of the 2100- $\text{cm}^{-1}$  band measured in the  $\{\bar{x}[z',y']x\}$  geometry is caused by a slight misalignment of the sample, which in an ideal case should be zero according to the selection rules of the fully symmetric representation of a trigonal defect. In the following discussion, we consider only the value of  $\Delta_{[100]}$  because both the 2100- and 4160- $\text{cm}^{-1}$  bands, regardless of the conditions of the sample preparation, display  $\Delta_{[110]} = 0$ .

As follows from Fig. 1,  $\Delta_{[100]}$  of the 2100- $\text{cm}^{-1}$  band is close to one, whereas Heyman *et al.* reported  $\Delta_{[100]} \cong 0.3$ . Another striking feature is that the 2100- and 4160- $\text{cm}^{-1}$  bands have precisely the same polarization properties. This may lead to the conclusion that  $\text{H}_2$  is aligned along the

[111] axis. However, this assignment meets with serious difficulties.

The first problem is that, according to theory, even interstitial  $\text{H}_2$  (at the  $T$  site) is a nearly free rotator [12,13].  $\text{H}_2$  in platelets should be much more isolated from the surrounding crystal and thus display the properties of a free rotator as well. It is difficult to envision a hindering potential strong enough to align the molecule along the [111] axis in the platelet.

The second problem with the suggestion of aligned  $\text{H}_2$  comes from the value of  $\Delta_{[100]}$ . From the known Raman tensor of free  $\text{H}_2$  [14],  $\Delta_{[100]}$  should equal 0.021, well below our observed value  $\Delta_{[100]} \cong 1$  for the 4160- $\text{cm}^{-1}$  line. In contrast, our polarized Raman data on the 3601- $\text{cm}^{-1}$  band associated with  $\text{H}_2$  at the  $T$  site are consistent with free  $\text{H}_2$ . The 3601- $\text{cm}^{-1}$  line is always polarized along the excitation light (see the inset of Fig. 1).

The data presented in Fig. 1 can be explained if we model the platelet as a flat thin dielectric layer ( $d \ll \lambda$ , where  $\lambda$  is the wavelength) described by an isotropic, frequency-independent, real dielectric constant  $\epsilon$ . This model takes into account (i) the interactions between scattering centers, i.e., Si—H bonds or  $\text{H}_2$ , and (ii) the change in the direction and intensity of the local electric field within the platelet from that of the incident electric field in the bulk of the sample.

According to the formalism proposed by Reed *et al.* [15], the local electric field in the platelet,  $\mathbf{E}^{\text{loc}}$ , expressed via the  $s$  and  $p$  polarization of the incident electric field,  $\mathbf{E}^{\text{in}}$ , may be written as

$$\mathbf{E}^{\text{loc}} = \mathbf{A}\mathbf{E}^{\text{in}} = \begin{pmatrix} 0 & f_x(\theta_{\text{in}}, \omega_{\text{in}}) \\ f_y(\theta_{\text{in}}, \omega_{\text{in}}) & 0 \\ 0 & f_z(\theta_{\text{in}}, \omega_{\text{in}}) \end{pmatrix} \begin{pmatrix} E_s^{\text{in}} \\ E_p^{\text{in}} \end{pmatrix}. \quad (1)$$

The functions  $f_i$  relate the electric field in the bulk of the sample to the platelet field and are functions of (a) the polar angle  $\theta_{\text{in}}$  measured with respect to the platelet normal, (b) the frequency of the excitation light, the incident frequency  $\omega_{\text{in}}$ , and (c) the dielectric constant  $\epsilon$ . The induced polarization  $\mathcal{P}^i$  of the oscillating Raman dipole is related to the local macroscopic electric field through the Raman tensor of the scatterer  $\alpha^i$ ,  $\mathcal{P}^i = \alpha^i \mathbf{E}^{\text{loc}}$ , where  $i$  is either Si—H or  $\text{H}_2$ . If  $z$  is the bond axis, then  $\alpha^i$  is diagonal and  $\alpha_{xx}^i = \alpha_{yy}^i = \delta^i$ ,  $\alpha_{zz}^i = 1$ , where  $\delta^i$  is the bond anisotropy defined as the ratio of the dynamic molecular polarizabilities perpendicular and parallel to the bond axis. Thus, the scattered electric field in the bulk of the sample,  $\mathbf{E}^{\text{sc}}$ , which is related to the induced polarization  $\mathcal{P}^i$  with frequency  $\omega_{\text{sc}}$  in the direction  $\theta_{\text{sc}}$  with respect to the platelet normal, is given by

$$\begin{pmatrix} E_s^{\text{sc}} \\ E_p^{\text{sc}} \end{pmatrix} = \frac{\omega_{\text{sc}}^2}{c^2} \mathbf{A}^T(\theta_{\text{sc}}, \omega_{\text{sc}}) \mathcal{P}^i, \quad (2)$$

where  $A^T$  is the transpose of  $A$ . Finally, the intensity of the appropriate Raman band,  $I_i$ , is given by

$$I_i \propto \sum_{k \in \{111\}} |e^{sc} A^T(\theta_{sc}^k, \omega_{sc}) \alpha^i A(\theta_{in}^k, \omega_{in}) e^{in}|^2, \quad (3)$$

where the summation is over the four possible orientations of the  $\{111\}$  platelet in the lattice. Here,  $e^{in}$  and  $e^{sc}$  are polarization vectors of the incident and scattered light, respectively. In case of  $H_2$ , Eq. (3) is averaged over all possible orientations of the principal axes of  $\alpha^{H_2}$  with respect to the laboratory frame, whereas for the  $2100\text{-cm}^{-1}$  band we assume that the Si—H bonds are aligned along the platelet normal.

$\Delta_{[100]}$  calculated from Eq. (3) for the  $2100\text{-cm}^{-1}$  and  $4160\text{-cm}^{-1}$  bands as a function of  $\epsilon$  is shown in Fig. 2. The dotted line indicates the dielectric constant of Si at  $488\text{ nm}$ . In our calculations we assumed that the Raman tensor of  $H_2$  is the same as that of the free molecule,  $\delta^{H_2} = 0.66$  [14], whereas for the  $2100\text{-cm}^{-1}$  band we used the value of the Si—H bond anisotropy  $\delta^{Si-H} = 0.35$ , obtained from the Raman study of vacancy-hydrogen defects in Si [16].

Thus, the polarization properties of the  $2100\text{-cm}^{-1}$  and  $4160\text{-cm}^{-1}$  bands presented in Fig. 1 can be explained if the platelet has a dielectric constant well below that of bulk Si. This is expected for the  $[2Si-H]_n$  structure. Indeed, this model assumes that  $[2Si-H]_n$  comprises two hydrogenated Si(111) layers with  $H_2$  trapped in between.

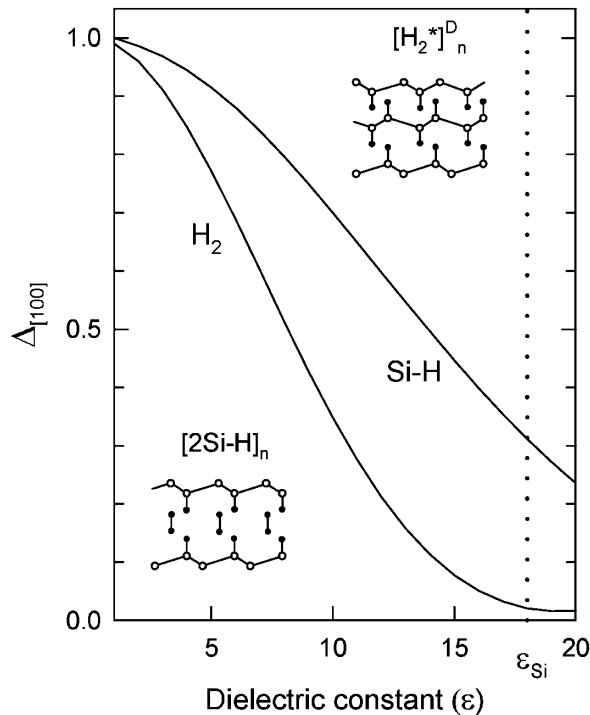


FIG. 2. Calculated depolarization ratio,  $\Delta_{[100]}$ , of the Si—H ( $2100\text{ cm}^{-1}$ ) and  $H_2$  ( $4160\text{ cm}^{-1}$ ) Raman signals. The dotted line shows the dielectric constant of Si at  $488\text{ nm}$ . The insets sketch the structures of the  $[H_2^*]^D_n$  and  $[2Si-H]_n$  platelets.

From the Fourier-transform infrared absorption studies, it has been found that the hydrogenated Si(111) surface has  $\epsilon = 2$  [17]. As the lattice dilates,  $\epsilon$  should decrease even more due to the bigger volume of the structure.

Figure 3 shows the integrated intensities and  $\Delta_{[100]}$  for the  $2100\text{-cm}^{-1}$  and  $4160\text{-cm}^{-1}$  bands as a function of the sample temperature during the plasma treatment.  $\Delta_{[100]}$  of the  $4160\text{-cm}^{-1}$  band remains constant whereas, at  $50^\circ\text{C}$ ,  $\Delta_{[100]}$  of the  $2100\text{-cm}^{-1}$  band is  $\approx 0.5$ . As the temperature rises, the  $4160\text{-cm}^{-1}$  band grows up and, when it reaches the maximal intensity, the  $2100\text{-cm}^{-1}$  band becomes nearly depolarized. We interpret this behavior as a transition of the platelet from the optical dense structure *without*  $H_2$  to the  $[2Si-H]_n$  structure *with*  $H_2$  in the interstitial region of the platelet. Indeed, according to Fig. 2,  $\Delta_{[100]} = 0.5$  for the  $2100\text{-cm}^{-1}$  band corresponds to  $\epsilon \approx 14$ , which is close to the dielectric constant of bulk Si. We want to point out that this transformation may be monitored only through the value of  $\Delta_{[100]}$ , because both the  $2100\text{-cm}^{-1}$  and  $4160\text{-cm}^{-1}$  bands are very broad and do not allow the resolution of changes in the poorly resolved fine structure.

The double layer of  $[H_2^*]^D_n$  is the most plausible candidate proposed thus far for the structure with  $\epsilon \approx 14$ . Of all suggested models for the  $\{111\}$  platelets, only the  $[H_2^*]^D_n$  one is expected to have the highest value of  $\epsilon$  (see the inset of Fig. 2). Simple estimates of  $\epsilon$  based on the

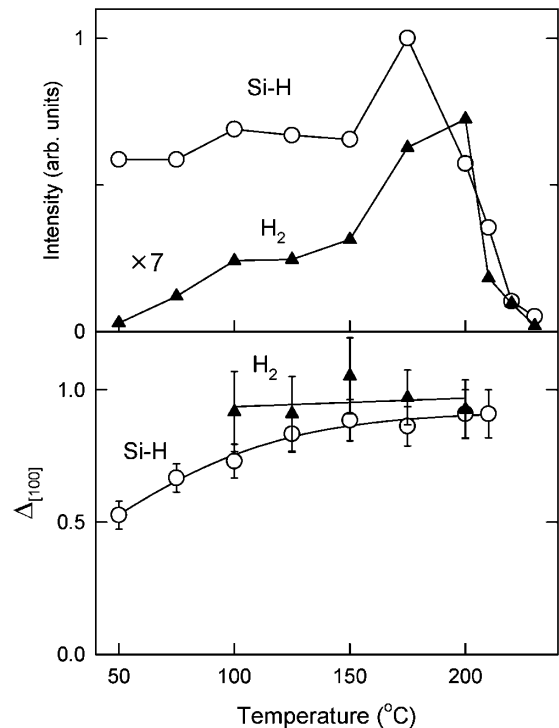


FIG. 3. Dependence of the integrated intensities (top figure) and the depolarization ratio,  $\Delta_{[100]}$  (bottom figure), of the Si—H ( $2100\text{ cm}^{-1}$ ) and  $H_2$  ( $4160\text{ cm}^{-1}$ ) Raman signals on sample temperature during hydrogen plasma treatment. The intensity of the Raman signal of  $H_2$  was scaled up by a factor of 7.

Lorentz-Lorenz formula [18] give  $\epsilon = 11$  if we assume that the lattice is dilated by 1 Å, compared to  $\epsilon = 2$  calculated for  $[2\text{Si—H}]_n$  with  $\text{H}_2$ . This platelet structure is in agreement with the recent calculations of Kim and Chang [19], who found that  $[\text{H}_2^*]_n^D$  has the lowest formation energy at small lattice dilations. Based on first-principle calculations, they showed that  $[\text{H}_2^*]_n^D$  is the most stable configuration of  $\text{H}_2^*$  aggregates stabilized due to strain release, as the lattice is dilated. For further lattice dilations, they found that  $[\text{H}_2^*]_n^D$  could turn into  $[2\text{Si—H}]_n$  with the formation of  $\text{H}_2$  in the interstitial region of platelets. From Fig. 3, the structural change occurs at 100 °C. Our data also explain the depolarization ratio of the platelet signal at 2100  $\text{cm}^{-1}$  obtained by Heyman *et al.* With the reported value of  $\Delta_{[100]} \cong 0.3$ , their samples should contain mainly the  $[\text{H}_2^*]_n^D$  structures.

In summary, we presented polarized Raman scattering spectra measured on  $\{111\}$ -hydrogen-induced platelets in Si hydrogenated by remote plasma. Our analysis of the Raman bands assigned to the  $\{111\}$  platelet identifies two different structures, which coexist in concentrations depending on the plasma conditions. Our data are in good agreement with recent theoretical calculations, where the  $[\text{H}_2^*]_n^D$  structure formed at low temperatures transforms into the  $[2\text{Si—H}]_n + \text{H}_2$  one as the temperature rises above 100 °C.

E. V. L. acknowledges the Alexander von-Humboldt Foundation for financial support and the Russian Foundation for Basic Research (Grant No. 99-02-16652).

---

\*Also at Institute of Radioengineering and Electronics, Mokhovaya 11, 103907 Moscow, Russia.

[1] *Hydrogen in Semiconductors*, edited by J. I. Pankove and N. Johnson, Semiconductors and Semimetals Vol. 34 (Academic Press, San Diego, 1991).

- [2] S. J. Pearton, J. W. Corbett, and M. Stavola, *Hydrogen in Crystalline Semiconductors* (Springer-Verlag, Berlin, 1992).
- [3] N. M. Johnson, F. A. Ponce, R. A. Street, and R. J. Nemanich, Phys. Rev. B **35**, 4166 (1987).
- [4] S. Muto, S. Takeda, and M. Hirata, Philos. Mag. A **72**, 1057 (1995).
- [5] J. N. Heyman, J. W. Ager III, E. E. Haller, N. M. Johnson, J. Walker, and C. M. Doland, Phys. Rev. B **45**, 13 363 (1992).
- [6] C. G. Van de Walle, P. J. H. Denteneer, Y. BarYam, and S. T. Pantelides, Phys. Rev. B **39**, 10 791 (1989).
- [7] P. Deák, C. R. Ortiz, L. C. Snyder, and J. W. Corbett, Physica (Amsterdam) **170B**, 223 (1991).
- [8] N. H. Nickel, G. B. Anderson, N. M. Johnson, and J. Walker, Phys. Rev. B **62**, 8012 (2000).
- [9] S. B. Zhang and W. B. Jackson, Phys. Rev. B **43**, 12 142 (1991).
- [10] A. W. R. Leitch, V. Alex, and J. Weber, Phys. Rev. Lett. **81**, 421 (1998).
- [11] M. Cardona, in *Light Scattering in Solids II*, edited by M. Cardona and G. Güntherodt (Springer-Verlag, Berlin, 1982), pp. 19–178.
- [12] B. Hourahine, R. Jones, S. Öberg, R. C. Newman, P. R. Briddon, and E. Roduner, Phys. Rev. B **57**, 12 666 (1998).
- [13] S. K. Estreicher, K. Wells, P. A. Fedders, and Pablo Ordejón, J. Phys. Condens. Matter **13**, 6271 (2001).
- [14] C. M. Hartwig and J. Vitko, Jr., Phys. Rev. B **18**, 3006 (1978).
- [15] C. E. Reed, J. Giergiel, J. C. Hemminger, and S. Ushioda, Phys. Rev. B **36**, 4990 (1987).
- [16] E. V. Lavrov, J. Weber, L. Huang, and B. Bech Nielsen, Phys. Rev. B **64**, 035204 (2001).
- [17] P. Jakob and Y. J. Chabal, J. Chem. Phys. **95**, 2897 (1991).
- [18] M. Born and E. Wolf, *Principles of Optics* (Pergamon, New York, 1964).
- [19] Y.-S. Kim and K. J. Chang, Phys. Rev. Lett. **86**, 1773 (2001).